scientific reports

Check for updates

OPEN

Synthesis and swelling studies of modified chitosan smart hydrogels containing alkyl sulfonate anionic pendant groups as microparticles for insulin release

Sabikeh G. Azimi[1]✉, F. Mehdi Moosavi[2], Zahra Khoshbin[3,4], Neda Shakour[4,5] & Sohrab Kazemi[6,7]

The hydrogel system effectively delivered insulin, demonstrating its potential to overcome challenges associated with conventional injectable insulin therapies. This pioneering platform leverages smart hydrogels, known for their responsiveness to environmental cues such as temperature, pH, ionic strength, and concentration. Among the fabricated hydrogels, the M5 microparticle, characterized by the lowest cross-linking agent concentration (14%) and the highest propane sultone content used during its preparation, exhibited the greatest water uptake and swelling capacity. Swelling studies confirmed that hydrogel swelling behaviour is significantly influenced by both pH and temperature. Increasing pH leads to increased swelling due to electrostatic repulsion between sulfonate groups (SO_3^-). However, a decrease in the swelling rate was observed in alkaline environments after a certain period, attributed to the removal of sulfonate functional groups via the Hoffman elimination reaction. Concurrently, increasing temperature resulted in an elevated swelling rate, which is likely due to the disruption of intramolecular non-covalent bonds, including hydrogen bonds formed between carboxyl and hydroxyl groups within the hydrogel structure. In other words, elevated temperatures enhance swelling by weakening intramolecular non-covalent bonds and increasing the amount of free space within the hydrogel. The effectiveness of this smart hydrogel-based platform was further validated using insulin as a model drug. Studies indicated that the microparticle loading rate increases with increasing insulin concentration in the loading solution, although this increase becomes less pronounced at higher concentrations. A concentration of 10 IU was determined to be optimal for insulin loading. An investigation into the drug release mechanism from the prepared microparticles suggested a perturbed Fickian mechanism for insulin release based on the obtained diffusion profile. The loading efficiency (LE) for M5 microparticles containing suspended insulin was reported to be 66.03%. This system effectively addresses the challenges associated with conventional injectable insulin therapies, offering a promising approach for precise and sustained insulin release in the body. In summary, this study successfully developed a novel, biocompatible, and smart hydrogel for insulin delivery that responds to pH and temperature changes, leading to controlled drug release and potentially improved therapeutic outcomes compared to traditional methods.

Keywords Smart hydrogels, Chitosan, Insulin, Microparticles, Natural polymers

[1]Department of Chemistry, Faculty of Sciences, University of Birjand, Birjand, Iran. [2]Department of Organic Chemistry, Faculty of Chemistry, University of Mazandaran, Babolsar, Iran. [3]Pharmaceutical Research Center, Pharmaceutical Technology Institute, Mashhad University of Medical Sciences, Mashhad, Iran. [4]Department of Medicinal Chemistry, School of Pharmacy, Mashhad University of Medical Sciences, Mashhad, Iran. [5]Student Research Committee, Faculty of Medicine, Mashhad University of Medical Sciences, Mashhad, Iran. [6]Cellular and Molecular Biology Research Center, Health Research Institute, Babol, Iran. [7]Neuroscience Research Center, Health Research Institute, Babol University of Medical Sciences, Babol, Iran. ✉email: sabikehazimi@gmail.com

Diabetes as a metabolic disease (fuel and food metabolism) is one of the most common diseases that are caused by the dysfunction of insulin hormone [1]. Factors contributing to diabetes includes race, lifestyle, and diet [2,3]. Inactivity and excessive calories consumption are primary contributors. The three main types of diabetes are type 1 (T1D), type 2 (T2D), and gestational diabetes [4,5]. In this disease, the immune system weakens, leading to elevated blood glucose levels and the further growth of the virus [6]. This increased glucose level further enhances the risk of viral infections, including Covid-19 [7,8]. Other serious complications associated with diabetes include diabetic ketoacidosis [9], neuropathy [10], eye damage [11] such as retinal damage and glaucoma, muscle complications [11] (leading to leg amputation), kidney failure, and cardiovascular diseases [12–16]. Individuals with T1D, T2D, and gestational diabetes can manage their blood glucose levels by taking insulin [17]. Insulin, the primary pancreatic hormone [18], is a globular protein consisting of two polypeptide chains linked by dual disulfide bonds [19]. Insulin is available in two pure forms with additives. The standard method for insulin administration in diabetes treatment is subcutaneous injection [13,20]. However, this approach presents drawbacks such as skin redness [21], pain, burning, and itching [22], and requires multi-phase administration with large doses [23]. Insulin's complex structure makes it sensitive to pH and temperature changes [24]. Furthermore, gastric enzymes (at pH 1.2–3.0) degrade insulin, rendering it ineffective for oral administration [25]. Therefore, insulin must be injected into the patient's body. To address these limitations and improve insulin treatment, enhancing its therapeutic efficacy, research has focused on polymer nanoparticles and nanoplatforms/carriers for the development of safe and efficient drug delivery systems as oral drugs [26,27]. One of the most important biomedical applications of nanomaterials is creating microgels, characterized by small particles sizes (100 nm diameter) and high-water swelling capacity [28]. In recent studies have highlighted the potential of hydrogels as drug delivery carriers due to their three-dimensional polymer networks [29–31] and the ability to retain water or biological fluids [32], especially when employed as stimuli-responsive sensor materials [33]. The pore size of microporous hydrogels is smaller than that of the gel network (ranging from 100 to 1000 nm), which enhances drug/protein stability and facilitates efficient drug loading, transport, and controlled release properties [34,35]. Depending on the preparation conditions and physicochemical properties, hydrogels exhibit unique characteristics [36]. Hydrogels can be of natural or synthetic origin and typically contain hydrophilic groups within their structure, including carboxylates (–COO–), amides ($CONH_2$), sulfonates (OSO_3^-), etc. [37]. They also have unique properties including sensitivity to temperature, pH, ionic strength and the concentration of specific substances in the environment [38–40]. Chitosan, one of the most abundant biopolymers on earth, holds significant potential for hydrogel preparation [41]. Chitosan is, a deacetylated chitin (with a degree of deacetylation higher than 50%), is highly valuable for therapeutic and medicinal applications due to its amine group. Chitosan possesses several advantageous properties, including biocompatibility, biodegradability, non-toxicity, non-immunogenicity, non-carcinogenicity, mucosal adhesion and antimicrobial activity without any known side effects making it widely used for drug delivery purposes [42]. Chitosan undergoes degradation through yeast reactions and finds specific application in the development of mucoadhesive formulations [43,44]. These formulations enhance the dissolution rate of poorly soluble drugs, improve drug targeting, and facilitate peptides absorption. Extensive chemical modifications have been employed to optimize the chemical-physical properties of chitosan [45,46]. It should also be noted that molecular weight and degree of deacetylation are important characteristics of chitosan because they affect its physicochemical properties and bioactivity. Also an important property of chitosan for oral drug delivery is its ability to open tight junctions between cells, increasing drug intestinal permeability. The limited solubility of chitosan hinders its application in combination with other polymers. Therefore, most of the chemical modifications focus on addressing this deficiency. The field of drug delivery using polymers and hydrogels has witnessed continuous progress due to its steady growth. Drug molecule release from a delivery system can occur through various mechanisms, including permeation, dissolution or decomposition, osmosis, and ion exchange. In this context, oral delivery systems, such as micro and nanoparticles composed of hydrophilic adhesive mucus, have gained significant importance for delivering of therapeutic proteins and peptides [47]. These mucoadhesive particles adhere to the stomach and intestinal walls extending their residence time within the gastrointestinal tract. Furthermore, these micro-particles enhance drug bioavailability by facilitating penetration through the mucosal barrier. They also protect drugs from enzymatic degradation, preserving the drug's integrity and ensuring direct delivery to the intestinal mucosa [48]. Chitosan, a promising polymer for oral drug delivery, offers a suitable route for drug delivery through the stomach and intestine. This is due to its biodegraded by stomach bacteria and its excellent bio adhesive properties [49,50]. Drug release from chitosan -based particle systems depend on factors such as the physicochemical properties of the drug, morphology, size, density of the particle system, as well as pH, polarity, and the presence of enzymes in the dissolution medium. The release of drugs from chitosan particle systems involves three distinct mechanisms: (a) release from the particle surface, (b) diffusion through the swollen rubber matrix, and (c) release due to polymer erosion [51]. Medicinal polymers offer several advantages over free drugs, including enhanced permeability and drug efficacy, extended half-life, ease of drug targeting to specific regions, improved penetration into cells with less cell resistance, reduced side effects, and maintenance of effective drug concentration in the bloodstream [52–56]. Various methods have been reported for the synthesizing chitosan-containing systems. The choice of method depends on several factors such as the desired particle size, thermal and chemical stability of active agent particles, and reproducibility of sample release kinetics, stability and toxicity of the final product [46].

This project, utilizing polymer chemistry and nanotechnology, investigates the synthesis of insulin drug carrier for the treatment of diabetes. Therefore, by making chitosan-based hydrogels with cross-links in the hydrogel with high elasticity, we succeeded in synthesizing the insulin drug carrier and releasing the drug in the intestine (at pH between 6.5 and 8.0) and increasing the percentage of drug absorption and eliminating insulin hydrolysis in the stomach and eliminating the disadvantages of injection.

Experimental section

Chemicals and devices

All reagents and solvents were purchased from Merck and Sigma-Aldrich, used without further purification. These included chitosan (Mw = 100,000–300,000), propane sultone (99%), citric acid monohydrate (Mw = 210.14), and sorbitan mono palmitate (span40).

Fourier-transform infrared (FT-IR) spectroscopy (model: Bruker Vector 22 spectrometer) using KBr pellets with Thermo spectrometer (scan range of 400–4000 cm^{-1}) was used to study structural changes in citric acid and propane sultone. Centrifuge Hettich Rotana (model: D7200), and Denley (model: BS 400), and freezer-dryer (model: FD-1 Eyela Tokyo Rikakikai) were employed during the synthesis process. UV/VIS spectrometer (model T90 +) was used measure the concentration insulin. A Metrohm pH meter (model pH Lab827) was used to determine of pH effect on swelling.

Field Emission Scanning Electron Microscopy (FESEM): TESCAN MIRA II microscope (20 kV accelerating voltage) equipped with a back-scattered electron (BSE) and elemental mapping was used to evaluate particle size and differentiate between nanoparticles with and without loaded insulin. Prior to FESEM imaging, samples were coated with a thin layer of gold using a vacuum sputter coater. X-ray Diffraction (XRD): A Bruker D8 Advance instrument (Karlsruhe, Germany) was used to obtain structural information about crystalline and amorphous materials. The instrument operated at 40 kV, 40 mA using Cu Kα radiation with a secondary monochromator.

Preparation of microparticles

First, we succeeded in synthesizing chitosan microparticles from the reaction of chitosan with acetic acid solution, and then, with sorbitan mono palmitate (SPAN 40) solution as a surfactant. Next, we synthesized the desired hydrogel by adding propane soltone to the solution of chitosan microparticles. In the last step, insulin was loaded as a model drug into the hydrogel (Scheme 1).

Briefly, chitosan (0.5 g) was dissolved in 25 ml of acetic acid solution 0.4% (v/v). This solution was added to 25 ml of 0.2% (v/v) sorbitan mono palmitate (SPAN 40) solution (as a surfactant). At the same time, it was stirred at 300–400 rpm by a magnetic stirrer at 60–65 °C. After 1 h, a cross-linking agent (14%, 28%, and 40% (w/w) citric acid to chitosan) was added dropwise to the solution. This solution was stirred for 24 h at 60 °C, and then, centrifuged at 2000–2500 rpm for two cycles of 15 min to separate chitosan microparticles (M1, M6, and M11 in Table 1). Propane sultone was added to the chitosan microparticle solution. This mixture was stirred at 300–400 rpm for 6 h at room temperature, and then, 0.5–1 ml of 10% sulfuric acid was added to it. Afterward, it was centrifuged at 2000–2500 rpm for two cycles of 15 min to achieve chitosan microparticles containing sulfonate (Scheme 1). Finally, all hydrogel was dried by freeze-drier at 0.4 Pa.

Drug loading efficiency

Suspend insulin-loaded M5 microparticle in 6 ml of phosphate buffer saline (pH = 7.4) at 37° C. At predetermined time intervals, remove samples of the release media. The centrifuge and filtered and filter the samples to extract the suspended microparticles. Afterward, the insulin concentration was measured by UV/ Vis spectrophotometer at 270 nm and 277 nm to compared the results with a calibration diagram. The loading efficiency was calculated using Eq. (1–2), and the results are reported in Table 2.

$$\mathrm{LE}\% = \text{ Theory value / Experimental value } \times 100 \tag{1-2}$$

Theory value: Measured drug concentration. Experimental value: Loaded drug concentration.

According to the studies for appropriate swelling, pH and temperature of about 25 °C (room temperature) were selected for loading drugs. The unit of measurement for insulin concentration is IU or International Unit. The amount of enzyme that can react or break down 1 micromole of substrate is called enzyme activity and is indicated by U or IU. The value of IU depends on temperature and pH. To evaluate the effect of drug concentration on loading, 5 IU, 10 IU, and 15 IU concentrations of insulin were prepared, and M5 microparticles was loaded in these insulin solutions within 24 h. After this time, the centrifuge solution was smooth by the micro-filter (to remove the micro porous that were suspended in the loading environment). The amount of the loaded drug was determined using UV/ Vis spectroscopy.

Sol–gel fraction studies

The sol–gel fraction was investigated in the synthesized smart hydrogels. For the determination of gel fractions were weighted 0.1 g of M1, M6, and M11 micro particles and then put on the pocket. Afterward, the micro particle was purified by water/ethanol mixture (100/25) at 100 °C for 24 h. According to Eq. (2–2), the gel fraction can be calculated by considering the weight ratio of the dried polymer (cross-linker (Wa)) and polymer after treatment with a solvent (Wb) (any appropriate ones for a polymer solvent).

$$\text{Gel fraction } \% = \mathrm{Wa/Wb} \times 100 \mathrm{Sol\ fraction}\ \% = 100 - \text{ gel fraction} \tag{2-2}$$

Swelling studies

This section details the investigation of swelling properties and *in-vitro* drug release behavior of the synthesized chitosan hydrogels. The swelling capacity of hydrogels were evaluated by immersing them in aqueous environments and calculating the swelling percentage using the following formula:

$$\text{Swelling } \% = \text{ Ws} - \mathrm{Wd/Ws} \times 100 \tag{3-2}$$

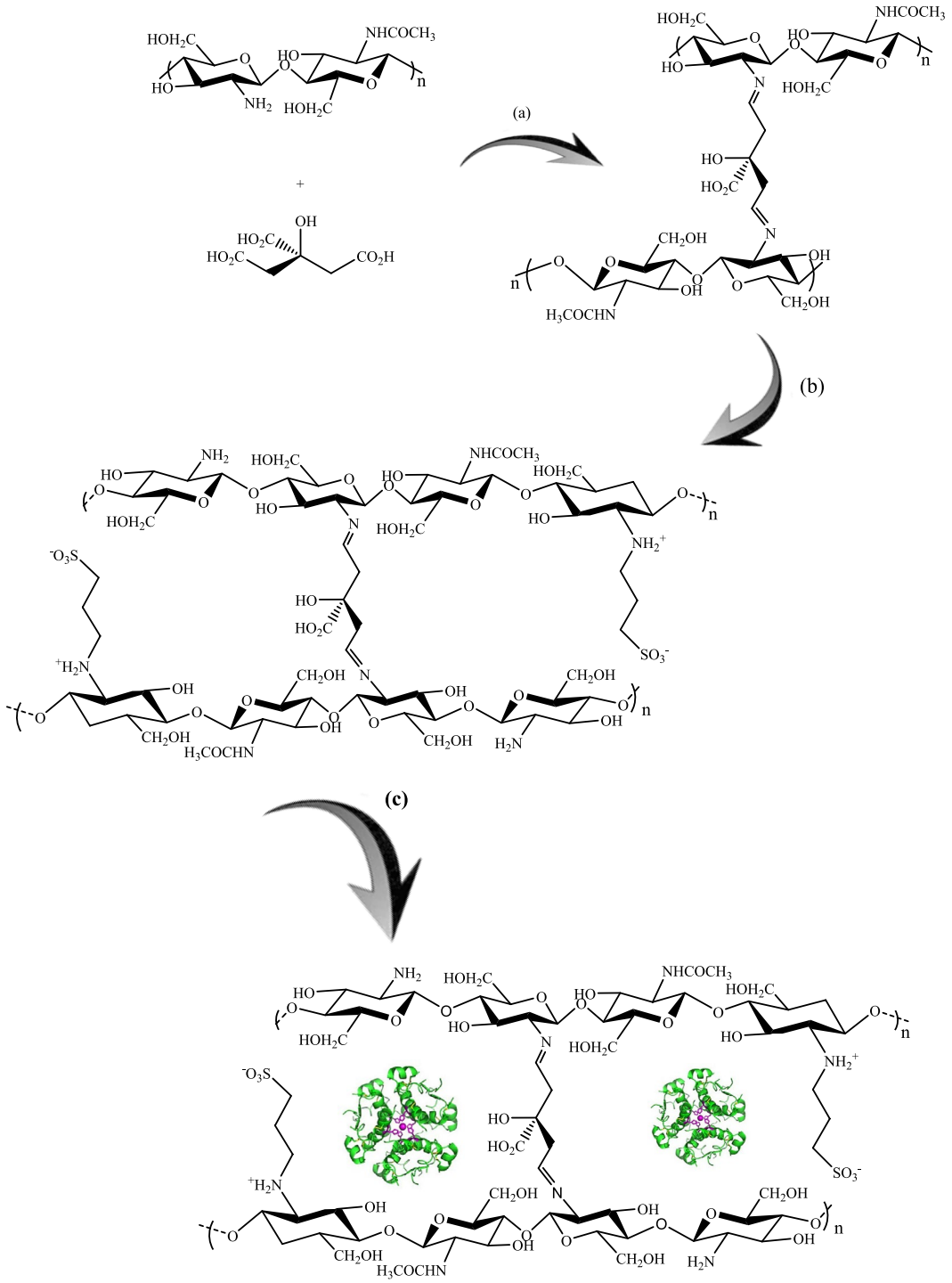

Scheme 1. Reagents and conditions for synthesis of the hydrogel and loading insulin into it: (**a**) 0.4% acetic acid, and 0.2% sorbitan mono palmitate, 24 h at 60 °C, Water. (**b**) propane sultone, 6 h at r.t, 10% sulfuric acid (**C**) Insulin (shown as a colored helix), phosphate buffer saline (pH = 7.4) at 37 °C.

Ws and Wd are the weight of the polymer in the swollen state and weight of the polymer in the dry state, respectively.

To determine the swelling degree, 0.1 g of micro particles was weighted and then placed in a container. Afterward, the container was immersed in a phosphate buffer solution at pH of 3, 7.4, and 9 at temperatures of 25 °C, 37 °C, and 60 °C. This allowed for the evaluation of the effect of pH and temperature on swelling.

Code	Citric acid (w/w %)	Propane sultone (M)	Code	Citric acid (w/w %)	Propane sultone (M)
M_1	14	0.0000	**M_9**	28	0.0046
M_2	14	0.0011	**M_{10}**	28	0.0068
M_3	14	0.0023	**M_{11}**	40	0.0000
M_4	14	0.0046	**M_{12}**	40	0.0011
M_5	14	0.0068	**M_{13}**	40	0.0023
M_6	28	0.0000	**M_{14}**	40	0.0046
M_7	28	0.0011	**M_{15}**	40	0.0068
M_8	28	0.0023			

Table 1. Formulation of the studied microparticle.

LE (%)	The amount of release after reaching the state of equilibrium (IU)	Loading rate in 0.1 g (IU)	The concentration of the drug used for loading (IU)	Code
66.03	1.72	62.2	10	M_5

Table 2. Loading efficiency checks.

In-vitro drug release studies

Insulin was loaded as a model drug into the modified chitosan hydrogels to investigate the drug loading and release behaviour by the swelling-diffusion approach. The release percentage of insulin was calculated using the following equation:

$$\text{Release}\% = \text{Wt}/\text{W}\infty \times 100 \quad (4\text{-}2)$$

where Wt and W∞ are the concentration released at time t and the total adsorbed insulin in the micro particle structure, respectively.

The loaded particles were placed in optimal conditions (pH, temperature, and concentration of the drug) in the release medium (saline phosphate buffer solution at 37 °C and pH = 7.4). At certain intervals, the release media was centrifuged and filtered. The sample absorption was measured using a UV/Vis spectrophotometer at two wavelengths of 270 and 277 nm, and the results were compared with a calibration curve. The release percentage was calculated by dividing the amount of drug released at each time point by the total loaded drug, and plotted as a release profile over time. In this study, compound M5 (consisting 14% cross-linking agent and 0.0068 mol of propane sultone), which exhibited the highest swelling capacity among the tested materials, was loaded with 10 IU of insulin in 24 h. The loaded particles were then placed in a saline phosphate buffer at pH = 7.4 and 37 °C. At designated time intervals, the microparticles were removed from the release environment, centrifuged, and the solution was filtered.

Investigation of drug release mechanism

The drug release calculated using the following equation:

$$\text{Mt}/\text{M}\infty = \text{ktn} \quad (5\text{-}2)$$

Mt/M∞ is the fractional drug release at time t, and k and n are a constant characteristic of the drug-polymer interaction and an empirical parameter characterizing the release mechanism, respectively. Based on the diffusion exponent (n), drug transport is classified as follows: Fickian (n = 0.5): Diffusion-controlled release. Case II transport (n = 1): Release dominated by polymer relaxation. Non-Fickian or Anomalous (0.5 < n < 1): A combination of diffusion and polymer relaxation. Super Case II (n > 1): Rapid release due to polymer chain movement.

n < 0.5 This range is typically associated with irregular-shaped particles and can decrease systematically with increasing cross-linking.

Results and discussions

Hydrogel characterization

FT-IR analysis

The structure of prepared microparticles was evaluated by FT-IR spectroscopy (Fig. 1A). In the following section, the infrared spectra of chitosan (a), chitosan crosslinked with citric acid (b), and chitosan crosslinked with citric acid and functionalized with soltone (c) are given. Depending on its degree of deacetylation, chitosan has a percentage of acetamide group in its structure. In the spectrum of chitosan, a peak at 1640 cm^{-1} is observed, corresponding to the carbonyl stretching vibration of the acetamide groups in chitosan. In the spectrum of chitosan cross-linked with citric acid, three peaks can be seen at 1640 cm^{-1}, 1710 cm^{-1}, and 1750 cm^{-1}. The peak at 1640 cm^{-1} is corresponds to the acetamide groups in the primary chitosan structure or the acetamide groups formed in the reaction between the amine groups of chitosan and carboxyl group of citric acid. A peak

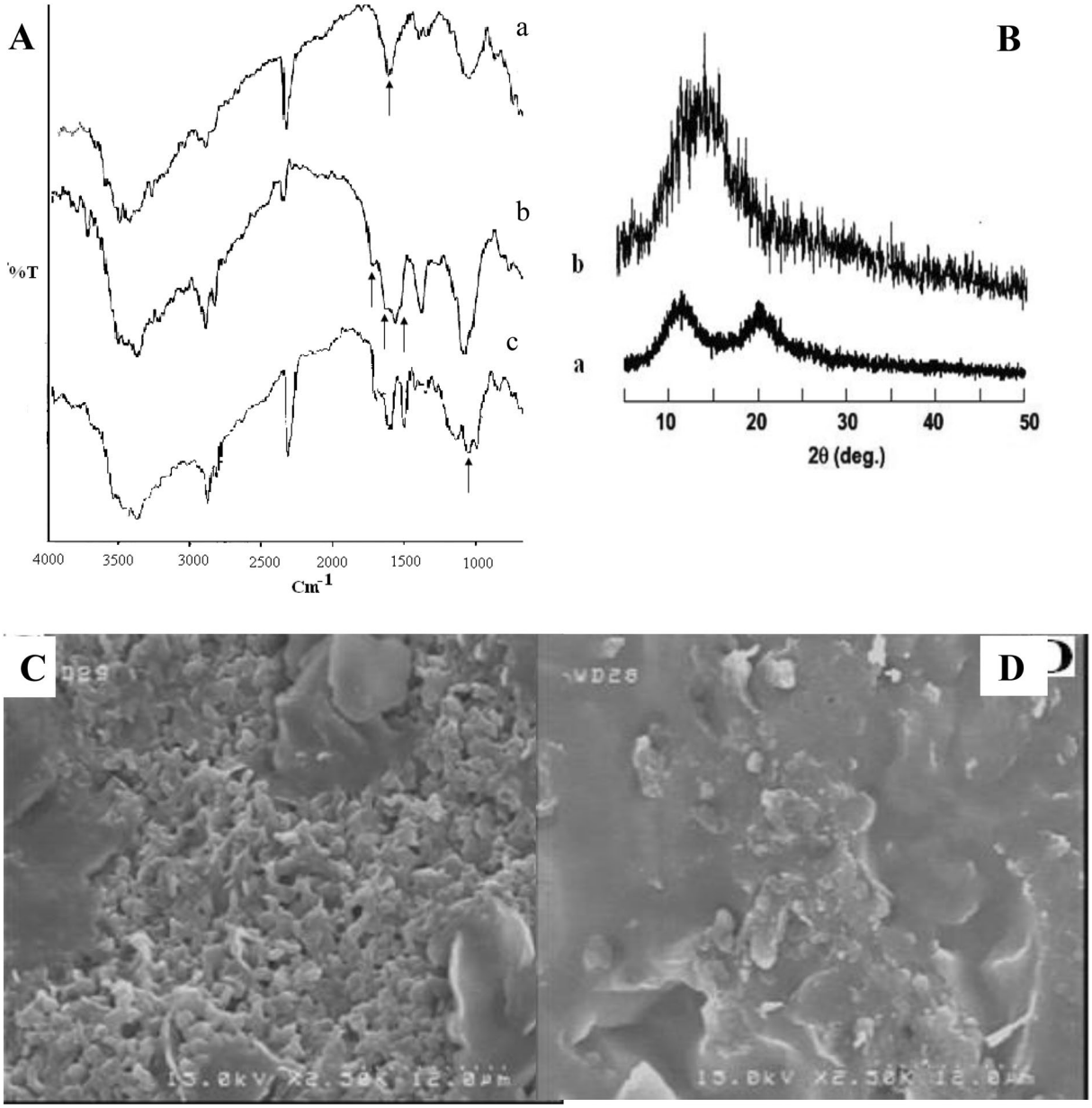

Fig. 1. (**A**) FT-IR Spectrum of chitosan (a), chitosan crosslinked with citric acid (b), and chitosan crosslinked with citric acid and functionalized with soltone (c). (**B**) XRD images of chitosan-containing sulfonate group (a), and pure chitosan (b). (**C**) SEM picture of the insulin-loaded nanoparticles. (**D**) SEM picture of the drug-free nanoparticles.

at 1710 cm^{-1} is related to carbonyl ester groups formed in the reaction between citric acid and hydroxyl groups of chitosan. The peak at 1750 cm^{-1} corresponds to the unreacted carboxylic acid groups of citric acid within the microparticle structure. The difference in the peaks between the wavelengths of 1000–1300 cm^{-1} is related to the appearance of stretching peaks associated with the sulfonate (SO_3^-) group.

XRD analysis

The XRD pattern of chitosan and cross-linked chitosan is depicted in Fig. 1B. Peaks at 2θ values of 10° and 20° with low-intensity crystalline areas are observed for chitosan containing a sulfonate group (a). A strong diffraction peak at 2θ of 15° is related to the crystal structure of pure chitosan, attributed to hydrogen bond interactions between hydroxyl groups (b). The amorphousness of the hydrogel is due to the bonding of the sulfonate group to the chitosan chain, leading to the destruction of intermolecular hydrogen bonds and crystalline regions after polymerization.

SEM analysis

The FE-SEM images of the synthesized particles are shown in Fig. 1C, D. It is evident that the particle size is in the nanometre range. Furthermore, the size difference between the loaded nanoparticles with insulin and drug-free nanoparticles is clear.

Gel fraction studies

The cross-linking reaction of chitosan with citric acid was performed by dissolving chitosan in an acetic acid solution, adding it to an aqueous solution containing the surfactant sorbitan monopalmitate, and then, increasing the citric acid monohydrate (at a specific concentration) in a controlled manner. The dependence of the gelation fraction on the cross-linking agent was investigated by changing the amount of citric acid monohydrate. Figure 2 indicates that adding citric acid as a cross-linking agent (from 14 to 40%) enhances the gel fraction, due to the increased cross-linking density. As shown in Fig. 2, an increase in the weight percentage of citric acid monohydrate to chitosan enhances the gel fraction. However, at higher concentrations, the slope of the graph decreases, indicating the gelation fraction does not reach 100%. The increase in the gel fraction with increasing the percentage of citric acid monohydrate to chitosan can be explained by the increased possibility of collision between adjacent chitosan chains and citric acid, leading to a greater number of transverse connections. This results in the formation of more interconnected networks.

Swelling studies

A crucial characteristic of all hydrogels is their ability to swell in aqueous environments or, in other words, to retain water/biological fluids within their polymer network. The ability to absorb and maintain these fluids without dissolving or losing the structural integrity is a key feature of synthetic hydrogels. The chemical structure of hydrogels and environmental characteristics are the most important factors influencing their swelling behavior. In the design of hydrogels, the response level, swelling, and deflation are the practical factors for drug delivery applications. For this purpose, the swelling property of hydrogels was evaluated. The swelling force is related to the elasticity of the hydrogel. When the swelling force equals the elastic force, the hydrogel swelling reaches equilibrium [57]. The amount of swelling has an opposite relationship with the number of cross-links: as the number of cross-links increases, the amount of swelling decreases. Network density is directly related to mechanical resistance and permeability. The mechanical properties of hydrogels depend on their type of hydrogel and their structure. Typically, hydrogels are mechanically weak due to their high-water content. While increasing the degree of cross-linking and copolymerization with hydrophobic comonomers can compensate for low mechanical strength, these factors also reduce swelling. In addition to the osmotic pressure in an aqueous environment, the strong interactions between the chemical structure of the hydrogel and the fluid (or, in other words, the tendency for mixing between the fluid and the polymer) drive the penetration of solvent molecules into the polymer. The opening of transverse links in the network creates a force that opposes the elastic pressure of the polymer chains. As swelling increases, the elastic pressure also increases until the two forces reach equilibrium, resulting in the hydrogel's maximum swelling. This study investigates relationship between the amount of cross-linking agent and propane sultone with the swelling rate. The effect of amount of cross-linking agent on the swelling rate is shown in Fig. 3A. The results indicate that as the amount of cross-linking agent increases from 14 to 40%, the cross-linking density increases while water absorption decreases. This is due to the reduction in free volume and empty spaces within the hydrogel, as well as the reduction of the mobility of

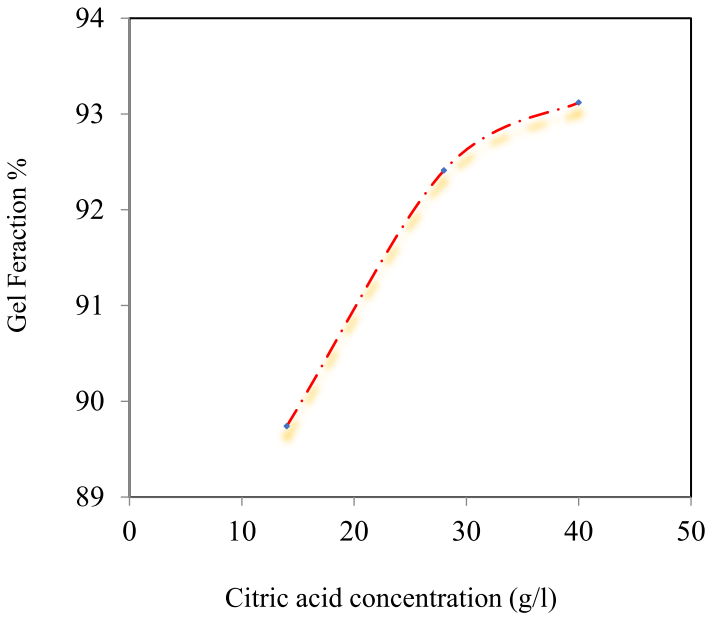

Fig. 2. Effect of the citric acid (%) (As a cross-linking agent) on the gel fraction (%).

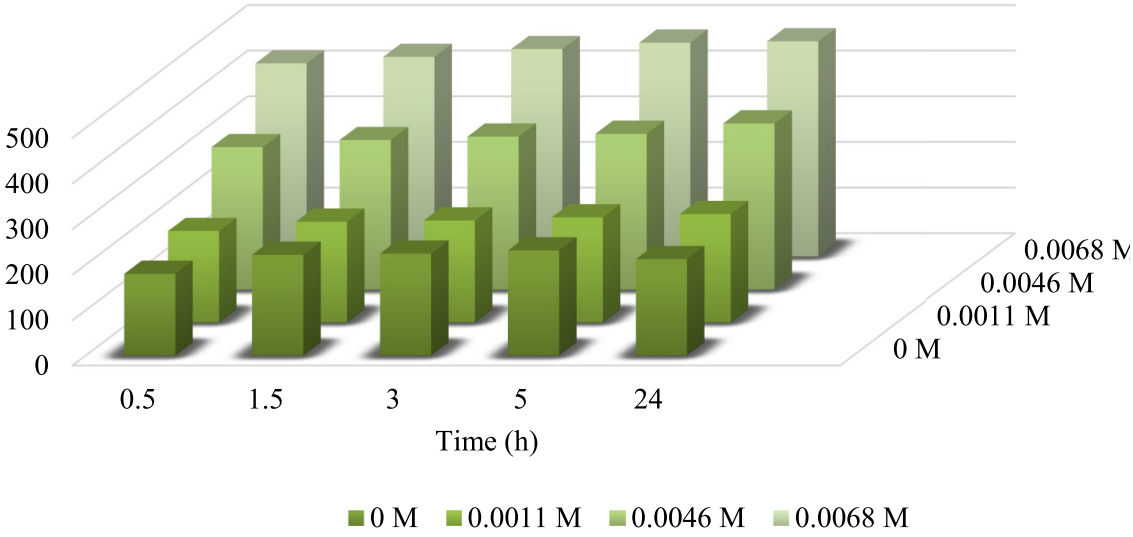

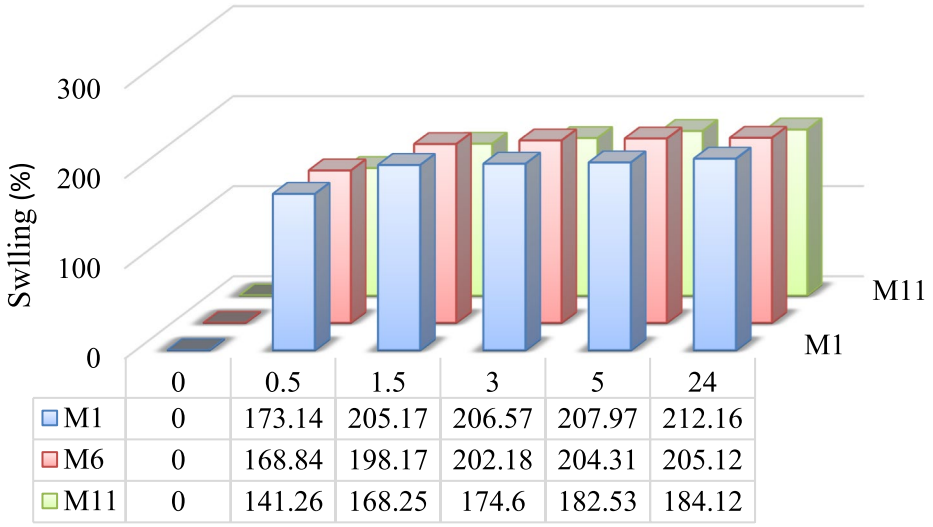

	0	0.5	1.5	3	5	24
M1	0	173.14	205.17	206.57	207.97	212.16
M6	0	168.84	198.17	202.18	204.31	205.12
M11	0	141.26	168.25	174.6	182.53	184.12

Fig. 3. Up graph: Comparison of the effect of different amounts of citric acid on the degree of swelling (%) (Fig. 3A), Down graph: Comparison of the effect of different amounts of propane sultone concentration (M) on the swelling of microparticles containing 14% cross-linking agent (Fig. 3B).

the networked polymer chains. Figure 3B displays the effect of amount of propane sultone on the swelling rate. Increasing the amount of propane sultone enhances swelling due to replacement of more hydrophilic ($-SO_3^-$) groups. Propane sultone (specifically, 1,3-propane sultone) is a cyclic ester of a sulfonic acid. Its ring is highly strained, making it a reactive electrophile. Chitosan, a deacetylated derivative of chitin, possesses abundant amine ($-NH_2$) and hydroxyl (–OH) groups. The interaction primarily occurs via ring-opening sulfonation by the amine groups on the chitosan polymer. Here's a detailed explanation:

1. Nucleophilic Attack: The lone pair of electrons on the nitrogen atom of the chitosan's amine group acts as a nucleophile and attacks the carbon atom of the propane sultone ring (specifically, the carbon next to the sulfur). This is an SN_2-type reaction.
2. Ring Opening and Sulfonation: The ring opens, breaking the C–O bond. This results in the formation of a sulfonate group ($-SO_3-$) attached to the nitrogen atom, forming a sulfobetaine structure. The reaction can be represented as follows:

$$\text{Chitosan} - \text{NH}_2 + \text{CH}_2\text{CH}_2\text{CH}_2\text{SO}_3 \rightarrow \text{Chitosan} - \text{NH}^+ - \text{CH}_2\text{CH}_2\text{CH}_2 - \text{SO}_3 -$$

3. Possible Side Reactions (Less Likely, but Possible): While the amine group is the primary site of reaction due to its higher nucleophilicity, hydroxyl groups (–OH) on the chitosan can also react with propane sultone, albeit to a lesser extent. This would result in sulfonation of the hydroxyl group:

$$\text{Chitosan} - \text{OH} + \text{CH}_2\text{CH}_2\text{CH}_2\text{SO}_3 \rightarrow \text{Chitosan} - \text{O} - \text{CH}_2\text{CH}_2\text{CH}_2 - \text{SO}_3\text{H}$$

4. Ionic Interactions: The sulfonate groups ($-SO_3^-$) introduced onto the chitosan backbone are negatively charged at neutral and alkaline pH. This creates a polyelectrolyte. These negative charges can then interact with:

* Cations in solution: The sulfonate groups can bind cations, leading to applications in heavy metal removal or controlled release of positively charged drugs.

* Positively charged sites on chitosan (if present): If the chitosan is not fully deacetylated, some acetylated units remain, which do not have the reactive amine group. Furthermore, at acidic pH values, some of the amine groups can become protonated (NH_3^+), leading to electrostatic interactions between the positively charged amine groups and the negatively charged sulfonate groups on the same or neighboring chitosan chains.

Further studies were conducted on made with 28% and 40% of cross-linking agents and different amounts of propane sultone. By plotting the swelling percentage of these micro particles against time, it was confirmed that increasing the amount of propane sultone during of particles increases the swelling percentage.

Effect of pH on swelling

Polymers with acidic or basic groups are pH-sensitive, meaning they can accept or lose protons in response to changes in environmental pH. In ionic hydrogels, pH changes lead to strong electrostatic repulsions between ionized groups and the rapid diffusion of water molecules. This results in the expansion of the polymer network of the designed smart hydrogels and acceleration of swelling. Hydrogels containing carboxylic acid or sulfonic acid groups are examples of this type of hydrogel. In these hydrogels, exceeding the environmental pH beyond the pKa of acidic groups leads to the dissociation of these groups. This event increases the number of anionic charges, enhancing electrostatic repulsion between groups and causing the hydrogel swells [58]. One environmental stimulus that significantly affects the water absorption of ionic hydrogels is the pH of the environment. In these hydrogels, ionic groups can dissociate in an aqueous environment due to pH changes, causing the hydrogel to swell due to the repulsion of ionic groups. Since the microparticles prepared by SO_3^- groups are pH-sensitive anionic hydrogels, the swelling rate of M5 hydrogel (the compound with the highest swelling rate among the 15 synthesized hydrogels) was investigated at pH values of 3, 7.4, and 9 at room temperature. Based on Fig. 4A, an increase in pH causes the dissociation of SO_3H groups and the repulsion by SO_3^- groups on the chains, which increases the swelling rate of fine particles. At pH values of 3 and 9, after reaching maximum swelling, the hydrogel starts to degrade after a certain period. The weight of the swollen microparticles decreases in acidic and alkaline environments.

The rate of water absorption is higher at a pH of 9, because SO_3H groups are converted to SO_3^- to a greater extent; However, in more alkaline environments, the destruction and removal of SO_3^- groups from the polymer chain occurs due to the Hoffmann elimination reaction (Scheme 2). This reduction in anionic groups on the polymer significantly decreases the number of absorption sites. In acidic and alkaline pH, the hemiacetal bonds in the hydrogel structure (formed in the reaction between citric acid and chitosan) break. Consequently, the weight decreases over time, and the swelling rate decreases (Fig. 4).

Effect of temperature on swelling

Some smart hydrogels change their water absorption due to temperature changes. When the hydrogel shrinks with increasing temperature, the hydrogen bond between the hydrophilic groups and water weakens. The interaction between the hydrophobic groups becomes dominant, causing the polymer chains to draw closer together. As a result, the hydrogel loses its water and becomes wrinkled [59]. However, some hydrogels swell with increasing temperature. These compounds are physically networked and contains many hydrophilic groups that form hydrogen bonds between the chain [60]. As the temperature increases, these hydrogen bonds are broken leading to a decrease in network density and an increase in water absorption. Another environmental stimulus affecting the water absorption in hydrogels is temperature. To investigate the effect of temperature on the water absorption rate of the prepared fine particles, the water absorption rate of the M5 compound was evaluated at room temperature, 37 °C, and 60 °C in double distilled water with pH≈7.4. The results of Fig. 4B, show that the water absorption of fine particles increases with rising the temperature. This increased water absorption can be attributed to the weakening and destruction of intramolecular non-covalent bonds, including hydrogen bonds. In fact, with the loss of these bonds create more free spaces for water penetration, increasing the water absorption capacity in the equilibrium state. According to the results, the prepared micro particles have positive temperature dependence. At a temperature of 60 °C, the weight of the swollen hydrogel gradually decreases after a few hours, reaching maximum swelling. Subsequently, swelling decreases due to the destruction of functional groups caused by the removal of Hoffmann.

Drug loading capacity

The drug loading capacity of M5 microparticles is presented in Table 3. Based on Table 3, the drug loading rate increases with increasing drug concentration. This is because the concentration difference allows for greater

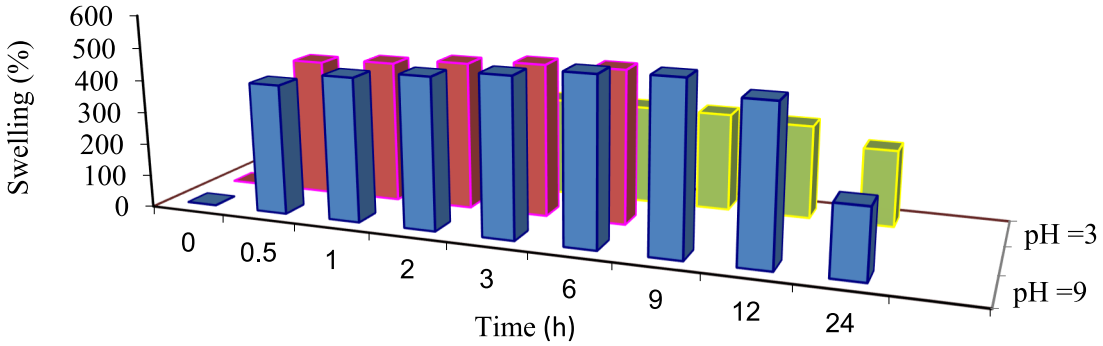

	0	0.5	1	2	3	6	9	12	24
pH =9	0	401.27	443.27	464.96	486.19	509.23	518.04	474.28	212.12
pH =7.4	0	422.85	437.14	454.28	468.57	471.42			
pH =3	0	276.21	284.38	296.17	302.24	301.15	300.15	286.22	233.13

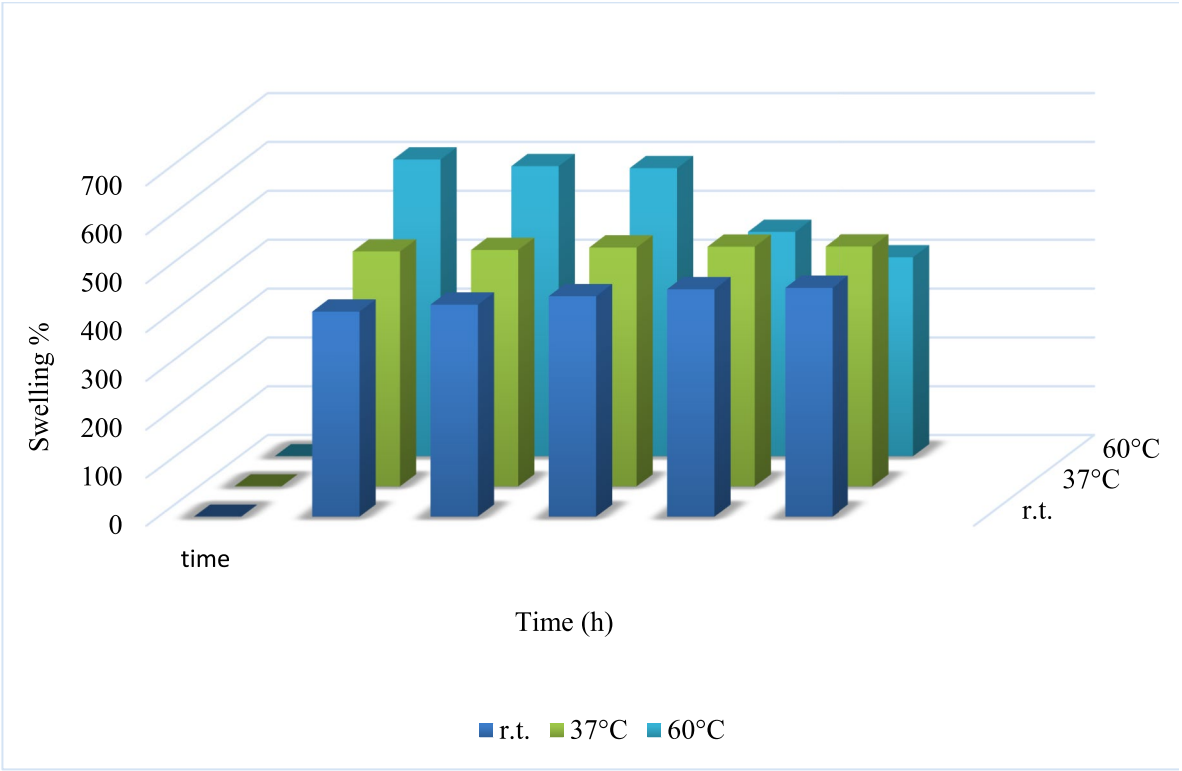

Fig. 4. Up graph: The effect of different pH on swelling of M5 microparticle (Fig. 4A). Down graph: The effect of different temperatures on swelling of M5 microparticle (Fig. 4B).

penetration of the drug into the microparticle's network structure. When the drug concentration exceeds a certain threshold, there is little difference in the amount of drug loaded. This is likely due to the filling of vacant spaces within the particle and approaching maximum loading capacity. Therefore, a 10 UI solution was selected for loading into the M5 hydrogel (prepared with 14% grid agent and 0.0068 mol propane sultone). Figure 5 illustrates the loading rate of M5 compound as a function of insulin solution concentration. It demonstrates that as the drug concentration increases, the loading rate also enhances. This is likely due to the enhanced concentration gradient driving force and increased penetration of insulin into the network structure of the fine particles. However, when the drug concentration exceeds a certain threshold, the loading rate plateaus. This saturation point reaches when the available spaces within the particles are filled, approaching the maximum loading capacity. Consequently, further increases in drug concentration result in negligible changes in the loading rate.

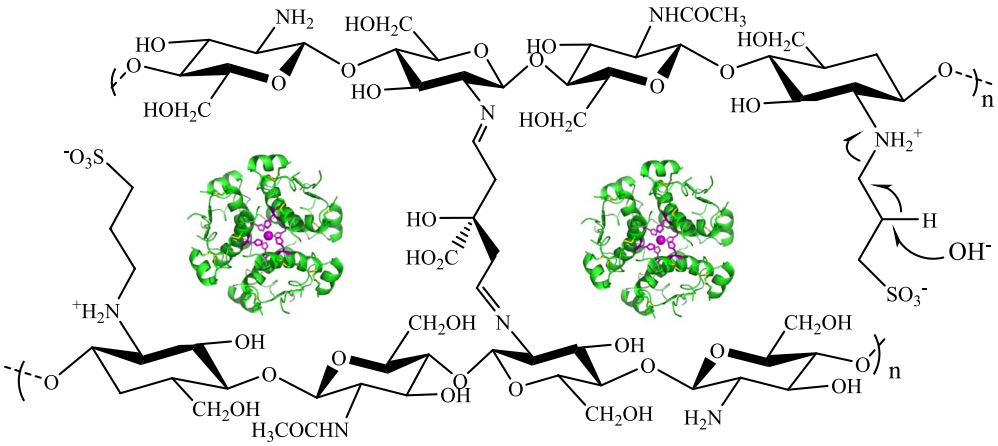

Scheme 2. The Hoffman elimination reaction.

Insulin concentration (IU) used for loading	Loading (IU) of micro particle
5	0.724
10	2.62
15	2.92

Table 3. The amount of loading obtained in different concentrations of insulin solution.

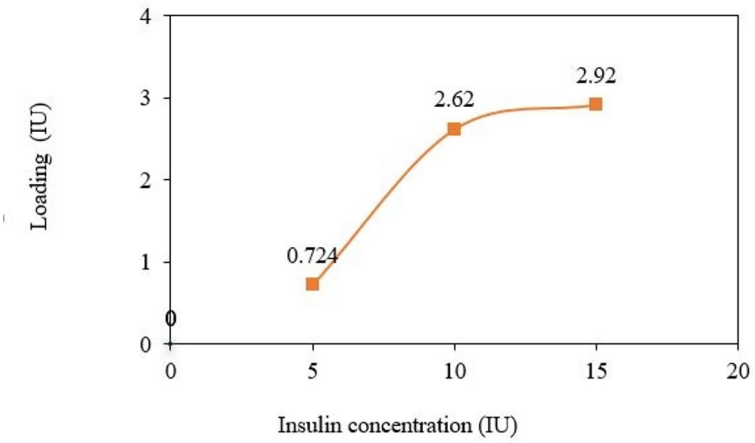

Fig. 5. Effect of different insulin concentrations on drug loading of the microparticle.

In-vitro drug release studies

The diagram of the insulin release as a function of time is shown in Fig. 6. Obviously, the drug release from the micro-particle is slowly and continuously for a long time, and the micro-particulates have a long period of activity.

Drug release mechanism

Data on drug release from M5 hydrogel (loaded with 10 IU insulin solution) at pH 7.4 and 37 °C were used to investigate the release mechanism. By plotting the log Mt/M∞ against the log T, the diffusion exponent (n) and the release constant (k) were calculated from the slope and y-intercept of the resulting linear regression, respectively. The obtained value of n = 0.415 indicates that the release mechanism deviates from Fickian diffusion (Fig. 7). This deviation can be attributed to the irregular shape of the prepared particles, which likely contributes to a more complex release profile. [61].

Conclusions

Chitosan is a polymer of glucose amine and N-acetyl glucose amine. This natural polymer has been considered as a drugs carrier, including its biocompatibility, biodegradability, adequate, and non-toxicity. But very low solubility

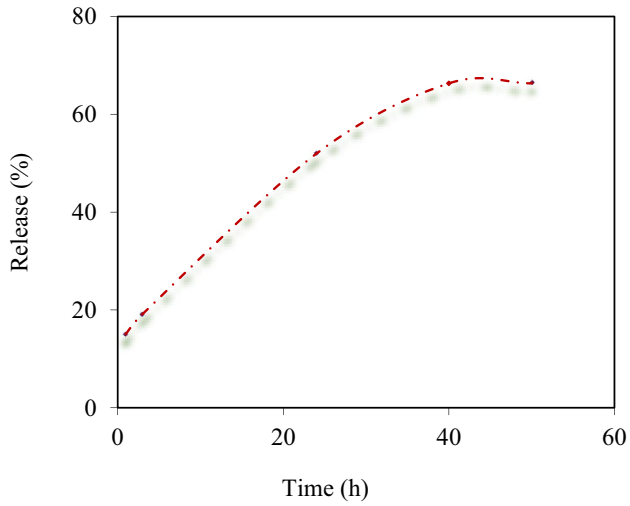

Fig. 6. The release profile of insulin from modified chitosan micro particle in PBS (pH 7.4 at 37° C).

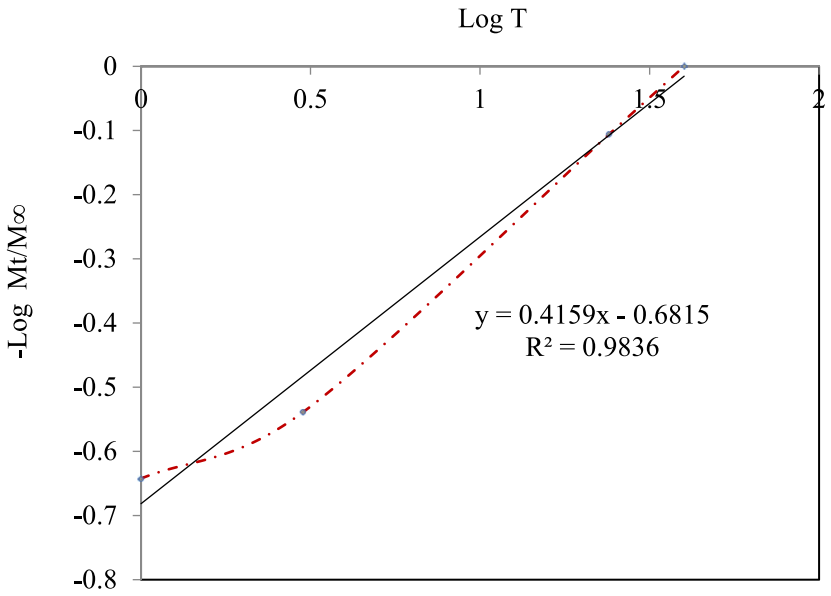

Fig. 7. Diagram of investigation of drug release mechanism.

in water limits the use of this valuable natural polymer in the medication. Various chemical modifications have been explored for chitosan to eliminate this weakness. The study addresses chitosan's low water solubility by using citric acid monohydrate and sulfonation to create physically strong and water-soluble particles. The M5 micro-particle exhibited the highest amount of networking agent, resulting in the highest water absorption and swelling among the synthesized hydrogels.

By changing pH of the environment, a dramatic change in the amount of particulate matter was observed. In alkaline environments, inflation decreased after a while, due to the elimination of sulfonate agents through the Hoffman elimination reaction. As the temperature risen, an increase in inflation was observed due to the failure of non-molecular bonds, including hydrogen bonds formed between carboxyl groups and hydroxyl in the hydrogel structure. Insulin was used as a model drug for diabetes treatment. The synthesized micro-particles were applied as the insulin carrier in extroversion tests. The results proved that the loading rate increased in the micro-particles with increasing insulin concentration. The insulin concentration of 10 UI was diagnosed for proper loading, and the drug release from the micronutrients was efficiently achieved.

Data availability

The datasets used and/or analysed during the current study available from the corresponding author on reasonable request.

Received: 12 February 2025; Accepted: 9 June 2025
Published online: 18 July 2025

References

1. Qaid, M. M. & Abdelrahman, M. M. Role of insulin and other related hormones in energy metabolism: A review. *Cogent Food Agric* **2**(1), 1267691 (2016).
2. Hu, F. B. Globalization of diabetes: the role of diet, lifestyle, and genes. *Diabetes Care* **34**(6), 1249–1257 (2011).
3. Shakour, N. et al. Antifibrotic effects of sodium-glucose cotransporter-2 inhibitors: A comprehensive review. *Diabetes Metab Syndr: Clin Res Rev* **18**(1), 102934 (2024).
4. Xiang, A. H. et al. Maternal gestational diabetes mellitus, type 1 diabetes, and type 2 diabetes during pregnancy and risk of ADHD in offspring. *Diabetes Care* **41**(12), 2502–2508 (2018).
5. Hoseinpoor, S. et al. PPARG modulation by bioactive compounds from Salvia officinalis and Glycyrrhiza glabra in type 2 diabetes management: A in silico study. *Innov Emerging Technol* **11**, 2450003 (2024).
6. Berbudi, A. et al. Type 2 diabetes and its impact on the immune system. *Curr. Diabetes Rev.* **16**(5), 442–449 (2020).
7. Erener, S. Diabetes, infection risk and COVID-19. *Mol Metab* **39**, 101044 (2020).
8. Azimi, S. et al. Green and rapid and instrumental one-pot method for the synthesis of imidazolines having potential anti-SARS-CoV-2 main protease activity. *Sustain Chem Pharm* **34**, 101136 (2023).
9. Curran, M.A., Diabetic ketoacidosis. Critical Care Obstetrics, 2024: p. 571–584.
10. Dillon, B. R., Ang, L. & Pop-Busui, R. Spectrum of diabetic neuropathy: New insights in diagnosis and treatment. *Annu. Rev. Med.* **75**(1), 293–306 (2024).
11. Srivastava, N., Chandra, M. & Nitesh,. Diabetes and the retinal changes in the eye: a threat to the sight. *Int J Community Med Public Health.* **11**(2), 1030 (2024).
12. Sharma, A. et al. Kidney and heart failure events are bidirectionally associated in patients with type 2 diabetes and cardiovascular disease. *ESC Heart Failure* **11**(2), 737–747 (2024).
13. Khoshbin, Z. et al. Aptamer-based biosensors: Promising sensing technology for diabetes diagnosis in biological fluids. *Curr Med Chem* **30**(30), 3441–3471 (2023).
14. Shakour, N. et al. Novel hits for targeting kidney failure in type 2 diabetes derived via in silico screening of the ZINC natural product database. *J Comput Sci* **85**, 102497 (2025).
15. Shakour, N. et al. Antioxidant effects of a novel pioglitazone analogue (PA9) in a rat model of diabetes: Modulation of redox homeostasis and preservation of tissue architecture. *J Diabetes Complicat* **38**(12), 108897 (2024).
16. Shakour, N. et al. Serum biochemical evaluation following administration of imidazolyl thiazolidinedione in streptozotocin-induced diabetic rats. *J Mol Histol* **55**(6), 1315–1325 (2024).
17. Jung, A. R. et al. Recent findings on exercise therapy for blood glucose management in patients with gestational diabetes. *J. Clin. Med.* **13**(17), 5004 (2024).
18. Lv, Y. et al. Differential diagnosis of post pancreatitis diabetes mellitus based on pancreatic and gut hormone characteristics. *J Clin Endocrinol Metab* **109**(8), 2003–2011 (2024).
19. Hidaka, K., et al., Advanced insulin synthesis by one-pot/stepwise disulfide bond formation enabled by S-protected cysteine sulfoxide. Chemistry: A European Journal, 2024: p. e202401003.
20. Zhao, R. et al. Drug delivery system in the treatment of diabetes mellitus. *Front Bioeng Biotechnol* **8**, 880 (2020).
21. Ahad, A. et al. Delivery of insulin via skin route for the management of diabetes mellitus: Approaches for breaching the obstacles. *Pharmaceutics* **13**(1), 100 (2021).
22. Demirağ, H., Hintistan, S. & Bulut, E. The effect of topically administered lavender aromatherapy on the pain of insulin injection in diabetic patients: A double-blind randomized controlled clinical trial. *Turk J Med Sci* **52**(6), 1845–1853 (2022).
23. Sehgal, S. et al. Use of a decision support tool and quick start onboarding tool in individuals with type 1 diabetes using advanced automated insulin delivery: A single-arm multi-phase intervention study. *BMC Endocr. Disord.* **24**(1), 167 (2024).
24. Richter, B., B. Bongaerts, and M.-I. Metzendorf, *Thermal stability and storage of human insulin.* Cochrane database of systematic reviews, 2023(11).
25. Safdar, R. & Thanabalan, M. Preparation of Chitosan-tripolyphosphate formulated insulin microparticles, their characterization, ANN prediction, and release kinetics. *J. Pharm. Innov.* **18**(3), 1047–1064 (2023).
26. Wang, Y. et al. Polymeric nanoparticles (PNPs) for oral delivery of insulin. *J Nanobiotechnol* **22**(1), 1 (2024).
27. Behzadifar, S. et al. Polymer-based nanostructures for pancreatic beta-cell imaging and non-invasive treatment of diabetes. *Pharmaceutics* **15**(4), 1215 (2023).
28. Heyns, I. M. et al. Glucose-responsive microgel comprising conventional insulin and curcumin-laden nanoparticles: A potential combination for diabetes management. *AAPS J.* **25**(4), 72 (2023).
29. Atia, G. A. N. et al. New challenges and prospective applications of three-dimensional bioactive polymeric hydrogels in oral and craniofacial tissue engineering: A narrative review. *Pharmaceuticals* **16**(5), 702 (2023).
30. Buwalda, S. J., Vermonden, T. & Hennink, W. E. Hydrogels for therapeutic delivery: Current developments and future directions. *Biomacromol* **18**(2), 316–330 (2017).
31. Ganguly, S. et al. Injectable and 3D extrusion printable hydrophilic silicone-based hydrogels for controlled ocular delivery of ophthalmic drugs. *ACS Appl. Bio Mater.* **7**(9), 6286–6296 (2024).
32. Samiraninezhad, N. et al. Using chitosan, hyaluronic acid, alginate, and gelatin-based smart biological hydrogels for drug delivery in oral mucosal lesions: A review. *Int J Biol Macromol* **252**, 126573 (2023).
33. Tian, B. & Liu, J. Smart stimuli-responsive chitosan hydrogel for drug delivery: A review. *Int. J. Biol. Macromol.* **235**, 123902 (2023).
34. Li, H. et al. Advances in the development of granular microporous injectable hydrogels with non-spherical microgels and their applications in tissue regeneration. *Adv Healthcare Mater* **13**(25), 2301597 (2023).
35. Das, P. et al. Borophene based 3D extrusion printed nanocomposite hydrogel for antibacterial and controlled release application. *Adv. Func. Mater.* **34**(21), 2314520 (2024).
36. Papagiannopoulos, A. et al. Physicochemical properties of electrostatically crosslinked carrageenan/chitosan hydrogels and carrageenan/chitosan/Laponite nanocomposite hydrogels. *Int. J. Biol. Macromol.* **225**, 565–573 (2023).
37. Ullah, F. et al. Classification, processing and application of hydrogels: A review. *Mater. Sci. Eng., C* **57**, 414–433 (2015).
38. Kurita, K. Chitin and Chitosan: Functional biopolymers from marine crustaceans. *Mar. Biotechnol.* **8**(3), 203 (2006).
39. Wandera, D., Wickramasinghe, S. R. & Husson, S. M. Stimuli-responsive membranes. *J. Membr. Sci.* **357**, 6–35 (2010).
40. Zhao, C. et al. Polymeric pH-sensitive membranes: A review. *Progr Polym Sci: PROG POLYM SCI* **36**, 1499–1520 (2011).
41. Boonsongrit, Y., Mitrevej, A. & Mueller, B. W. Chitosan drug binding by ionic interaction. *Eur J Pharm Biopharm* **62**(3), 267–274 (2006).
42. Salehi, E., Daraei, P. & Arabi Shamsabadi, A. A review on chitosan-based adsorptive membranes. *Carbohydr Polym.* **152**, 419–432 (2016).
43. Bhattarai, N., Gunn, J. & Zhang, M. Chitosan-based hydrogels for controlled, localized drug delivery. *Adv Drug Deliv Rev* **62**(1), 83–99 (2010).
44. Islam, A. et al. Controlled release of aspirin from pH-sensitive chitosan/poly(vinyl alcohol) hydrogel. *J. Appl. Polym. Sci.* **124**(5), 4184–4192 (2012).

45. Gzyra-Jagieła, K., et al., Physicochemical properties of chitosan and its degradation products, in chitin and chitosan. 2019. p. 61–80.
46. Timur, M. & Paşa, A. Synthesis, characterization, swelling, and metal uptake studies of aryl cross-linked chitosan hydrogels. *ACS Omega* **3**(12), 17416–17424 (2018).
47. Kumar, M. et al. Micro and nano-carriers-based pulmonary drug delivery system: Their current updates, challenges, and limitations—A review. *JCIS Open* **12**, 100095 (2023).
48. Lou, J. et al. Advances in oral drug delivery systems: Challenges and opportunities. *Pharmaceutics* **15**(2), 484 (2023).
49. Shafabakhsh, R. et al. Chitosan: A compound for drug delivery system in gastric cancer-a review. *Carbohyd. Polym.* **242**, 116403 (2020).
50. Sayed, S. & Jardine, A. Chitosan derivatives as important biorefinery intermediates Quaternary tetraalkylammonium chitosan derivatives utilized in anion exchange chromatography for perchlorate removal. *Int J Mol Sci.* **16**(5), 9064–9077 (2015).
51. Keawchaoon, L. & Yoksan, R. Preparation, characterization and in vitro release study of carvacrol-loaded chitosan nanoparticles. *Colloids Surf., B* **84**(1), 163–171 (2011).
52. Harrison, I. P. & Spada, F. Hydrogels for atopic dermatitis and wound management: A superior drug delivery vehicle. *Pharmaceutics.* **10**(2), 71 (2018).
53. Buwalda, S. J. et al. Hydrogels in a historical perspective: From simple networks to smart materials. *J Control Release* **190**, 254–273 (2014).
54. Peng, C., Zhao, Q. & Gao, C. Sustained delivery of doxorubicin by porous $CaCO_3$ and chitosan/alginate multilayers-coated $CaCO_3$ microparticles. *Colloids Surf., A* **353**(2), 132–139 (2010).
55. Anirudhan, T. S., Nima, J. & Divya, P. L. Synthesis, characterization and in vitro cytotoxicity analysis of a novel cellulose based drug carrier for the controlled delivery of 5-fluorouracil, an anticancer drug. *Appl. Surf. Sci.* **355**, 64–73 (2015).
56. Zhang, Y., Chan, H. F. & Leong, K. W. Advanced materials and processing for drug delivery: The past and the future. *Adv Drug Deliv Rev* **65**(1), 104–120 (2013).
57. Peppas, N. A. et al. Physicochemical foundations and structural design of hydrogels in medicine and biology. *Annu. Rev. Biomed. Eng.* **2**(1), 9–29 (2000).
58. Patel, V. R. & Amiji, M. M. Preparation and characterization of freeze-dried chitosan-poly(ethylene oxide) hydrogels for site-specific antibiotic delivery in the stomach. *Pharm. Res.* **13**(4), 588–593 (1996).
59. Brannon-Peppas, L. & Peppas, N. A. Dynamic and equilibrium swelling behaviour of pH-sensitive hydrogels containing 2-hydroxyethyl methacrylate. *Biomaterials* **11**(9), 635–644 (1990).
60. Khare, A. R. & Peppas, N. A. Release behavior of bioactive agents from pH-sensitive hydrogels. *J. Biomater. Sci. Polym. Ed.* **4**(3), 275–289 (1993).
61. Agnihotri, S. A. & Aminabhavi, T. M. Controlled release of clozapine through chitosan microparticles prepared by a novel method. *J Control Release* **96**(2), 245–259 (2004).

Acknowledgements

We are grateful to the research deputy of Babol University of Medical Sciences and Mazandaran University for the financial support and Birjand University and Mashhad University for conducting research.

Author contributions

Sabikeh G. Azimi , Mehdi Moosavi F were responsible for the laboratory and practical part of the article and writing the manuscript of the original text. Zahra Khoshbin , Neda Shakour, Sohrab Kazemi edited the manuscript of the original text.

Funding

This study was supported by the research deputy of Babol University of Medical Sciences and Mazandaran University [Grant Numbers: 4570].

Declarations

Competing interests

All authors declare that no conflict of interest exists.

Additional information

Correspondence and requests for materials should be addressed to S.G.A.